Magnetostructural phase transitions in $Ni_{50}Mn_{25+x}Sb_{25-x}$ Heusler alloys

2008 J. Phys.: Condens. Matter 20 235204

(http://iopscience.iop.org/0953-8984/20/23/235204)

J. Phys.: Condens. Matter **20** (2008) 235204 (8pp) doi:10.1088/0953-8984/20/23/235204

Magnetostructural phase transitions in $Ni_{50}Mn_{25+x}Sb_{25-x}$ Heusler alloys

Mahmud Khan[1], **Igor Dubenko, Shane Stadler and Naushad Ali**

Department of Physics, Southern Illinois University, Carbondale, IL 62901, USA

Received 18 December 2007, in final form 3 April 2008
Published 30 April 2008
Online at stacks.iop.org/JPhysCM/20/235204

Abstract

The structural and magnetic properties of $Ni_{50}Mn_{25+x}Sb_{25-x}$ ($0 \leqslant x \leqslant 18$) Heusler alloys have been investigated by x-ray diffraction, magnetization, thermal expansion, and electrical resistivity measurements. Austenitic phases with the $L2_1$ cubic crystal cell and martensitic phases with *Pmm2* orthorhombic structures have been observed at room temperature in alloys with $0 \leqslant x \leqslant 12.5$ and $13 \leqslant x \leqslant 14$, respectively. The Curie temperatures of the austenitic phases decrease linearly with increasing x and change from 370 ($x = 0$) to 340 K ($x = 12.5$). In the concentration $7 < x \leqslant 10$, the system is found to undergo martensitic phase transitions above 150 K. The martensitic transition temperatures increase rapidly with increasing x and for $x \geqslant 13.5$ the temperature exceeds the Curie temperature of the austenitic phase (340 K). The alloys in their martensitic phases exhibit complex magnetic behavior. The phase diagram with respect to temperature and composition of the $Ni_{50}Mn_{25+x}Sb_{25-x}$ system has been determined, where the following magnetic phases have been observed in the martensitic state: antiferromagnetic phase ($14 < x$); paramagnetic and antiferromagnetic ($13 \leqslant x \leqslant 14$, above 120 K) mixed phase; ferromagnetic and antiferromagnetic ($10 \leqslant x \leqslant 14$, above 20 K) mixed phase. The mixed phases result in observation of the exchange bias effect at low temperatures (below 120 K).

(Some figures in this article are in colour only in the electronic version)

1. Introduction

Among the first-order magnetostructural phase transitions in solid state physics, the martensitic transition is one of the most well known, and has been a subject of intense research interest for many years. The martensitic transition is a diffusionless solid–solid structural phase transition where the displacements of the neighboring atoms are smaller than the atomic separation. Recently, there has been much interest in materials that exhibit ferromagnetism and undergo martensitic transformations. The reason is that such materials exhibit shape memory effects that can be controlled by the application of external magnetic fields. Some Heusler alloys undergo martensitic phase transitions where both crystalline states, above and below the martensitic transformation, are ferromagnetic. The high temperature austenite phase possesses an $L2_1$ cubic structure, while the low temperature martensitic phase may have a tetragonal or orthorhombic structure [1–3]. Ni_2MnGa is the most well known ferromagnetic shape memory Heusler alloy, and has been the subject of much research in the last decade [4–9]. It has been an impetus for the development of new Heusler alloys that undergo martensitic transitions while in a ferromagnetic state.

Recently some non-Ga based Ni–Mn–X (X = In, Sn, Sb) Heusler alloys have been reported that undergo martensitic transformations while in a ferromagnetic state [10]. In their stoichiometric form of Ni_2MnX, the alloys do not exhibit any martensitic transformation. When X is partially replaced by Mn martensitic transitions are observed for some critical concentration. Studies of the magnetic and structural properties of $Ni_{0.50}Mn_{0.50-x}Sn_x$ and $Ni_{0.50}Mn_{0.50-x}In_x$ have been performed by some research groups [11–13]. It was shown that, in these alloy systems, the magnetic moments in the martensitic phases are lower than the moments in the austenitic phases [12]. From an application point of view, these alloy systems have already attracted much interest. Significant properties of these alloys, such as large magnetoresistance, magnetocaloric effects, and exchange bias properties have been reported [14–20]. Although the Ni–Mn–X (X = In, Sn, Sb) alloy systems are found to possess interesting properties

[1] Author to whom any correspondence should be addressed.

Table 1. Crystal structures and lattice parameters at room temperature of $Ni_{50}Mn_{25+x}Sb_{25-x}$ for the indicated value of concentration x.

x	Crystal structure	Space group	a (Å)	b (Å)	c (Å)	V (Å)^3	R_p	R_{wp}	R_{exp}	χ^2
0	$L2_1$ Cubic	$Fm\bar{3}m$	6.027(1)	6.027(1)	6.027(1)	218.93(1)	25.18	39.89	29.71	1.8
6	$L2_1$ Cubic	$Fm\bar{3}m$	6.018(1)	6.018(1)	6.018(1)	217.95(1)	18.74	24.23	25.48	0.9
7	$L2_1$ Cubic	$Fm\bar{3}m$	6.008(1)	6.008(1)	6.008(1)	216.87(1)	25.63	38.91	44.57	0.76
10	$L2_1$ Cubic	$Fm\bar{3}m$	5.992(1)	5.992(1)	5.992(1)	215.14(1)	24.25	36.64	42.86	0.73
12	$L2_1$ Cubic	$Fm\bar{3}m$	5.981(1)	5.981(1)	5.981(1)	213.95(1)	14.96	19.05	19.62	0.94
12.5	$L2_1$ Cubic	$Fm\bar{3}m$	5.980(1)	5.980(1)	5.980(1)	213.85(1)	22.42	29.79	15.70	3.6
13	Orthorhombic	*Pmm2*	4.289(1)	5.670(1)	21.564(1)	524.41(1)	14.99	19.92	22.20	0.81
13.5	Orthorhombic	*Pmm2*	4.296(1)	5.645(1)	21.474(1)	520.76(1)	13.96	18.44	20.73	0.79
14	Orthorhombic	*Pmm2*	4.303(1)	5.668(1)	21.467(1)	523.57(1)	30.66	45.59	35.92	1.61

from both scientific and application points of view, many aspects of their magnetic and structural properties are yet to be investigated.

In this work we present an experimental study on the off-stoichiometric Heusler alloy system $Ni_{50}Mn_{25+x}Sb_{25-x}$ ($0 \leqslant x \leqslant 14$). We have elucidated detailed magnetic and structural properties of this system through magnetization, x-ray diffraction, electrical resistivity, and thermal expansion measurements. The objective was to understand the basic properties of the magnetostructural transitions in this alloy system.

2. Experimental technique

Approximately 5 g polycrystalline $Ni_{50}Mn_{25+x}Sb_{25-x}$ ($0 \leqslant x \leqslant 18$) buttons were fabricated by conventional arc melting in an argon atmosphere using Ni, Mn, and Sb of 4N purity. Since Mn and Sb vaporize very easily, some excess of the elements (approximately 2% by weight of Mn and 0.4% by weight of Sb) were added to the stoichiometric amount to compensate for the mass loss during melting. The approximations of the extra weight were obtained by melting the individual elements separately followed by evaluation of the mass loss after melting. The elements were melted four times, and the weight loss after melting was found to be less than 0.2%. For homogenization, the samples were wrapped in tantalum foil and annealed in vacuum for 144 h at 850 °C, and slowly cooled down to room temperature.

For phase identification and the determination of lattice constants, x-ray diffraction (XRD) measurements were conducted at room temperature using a GBC MMA (Mini Materials Analyzer) x-ray diffractometer that used Cu Kα radiation and Bragg–Brentano geometry. The XRD patterns were analyzed and indexed using the Windows version of Powdercell XRD [21] and Fullprof [22] software.

The magnetization measurements were performed on a superconducting quantum interference device (SQUID) magnetometer manufactured by Quantum Design Inc. The measurements were performed in a temperature range of 5–400 K and in magnetic fields up to 50 kOe. Zero field cooled (ZFC) and field cooled (FC) magnetization measurements were performed in a field of 100 Oe. Before performing the ZFC measurements the samples were cooled from 400 to 5 K in zero magnetic field. Prior to the FC measurements, samples were cooled down from 400 to 5 K in an applied magnetic field of 100 Oe. The saturation magnetic moments (M_S) at 5 K were estimated from the M versus H^{-1} curves by extrapolating the curves to $H^{-1} = 0$.

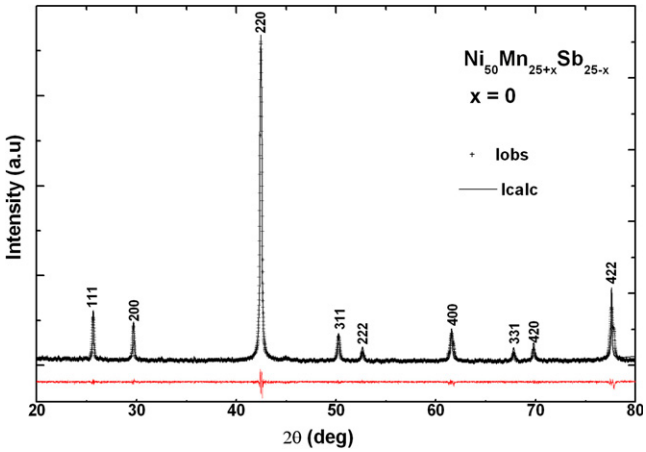

Figure 1. Room temperature observed and calculated powder XRD pattern of $Ni_{50}Mn_{25+x}Sb_{25-x}$ ($x = 0$).

Direct current resistivity, using the four-probe method, was measured over the same temperature range as the magnetization measurements. To eliminate the contribution of thermoelectric effects, the current direction was reversed and an average of the voltage drops in each direction was recorded. Thermal expansion measurements were performed using a high resolution capacitance dilatometry method in a temperature range of 100–350 K [23].

3. Experimental results

3.1. X-ray diffraction

The observed and calculated room temperature XRD patterns of $Ni_{50}Mn_{25+x}Sb_{25-x}$ ($x = 0$) are shown in figure 1. The XRD patterns indicate that the samples are in the austenitic phase and possess the Heusler $L2_1$ cubic structures belonging to the $Fm\bar{3}m$ space group. As shown in figure 2, all of the other $Ni_{50}Mn_{25+x}Sb_{25-x}$ samples, with x ranging from 6 to 12.5, possess cubic structures at room temperature. With increasing Mn content, the lattice constants of the austenitic phases are found to decrease (see table 1). This decrease of the lattice constants could be due to the fact that the atomic radius of Mn (1.40 Å) is smaller than Sb (1.45 Å).

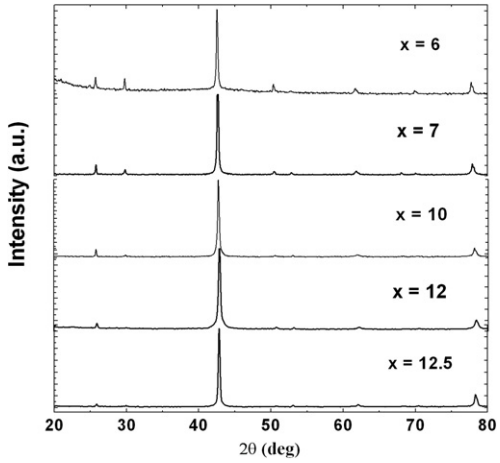

Figure 2. Room temperature powder XRD patterns showing the $L2_1$ phases of $Ni_{50}Mn_{25+x}Sb_{25-x}$.

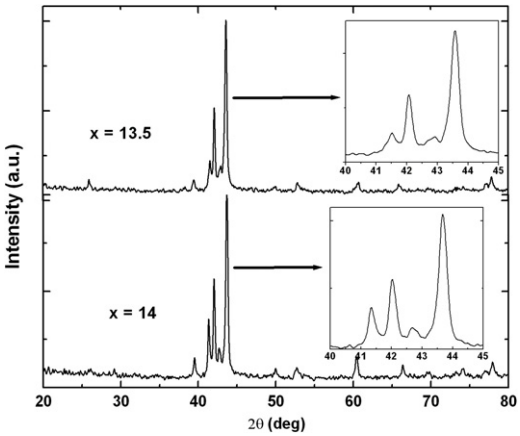

Figure 4. Room temperature powder XRD patterns showing the martensitic phases of $Ni_{50}Mn_{25+x}Sb_{25-x}$.

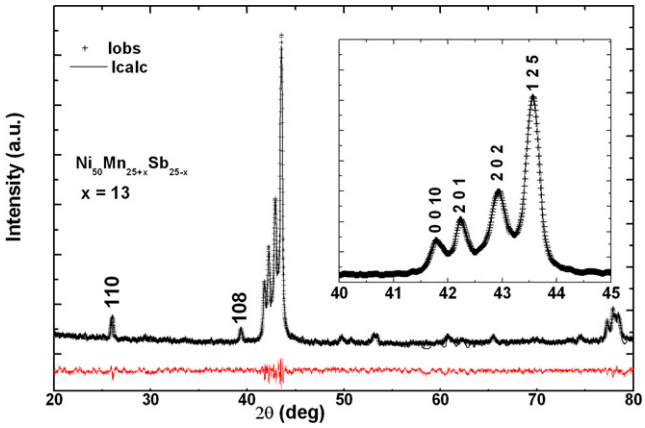

Figure 3. Room temperature powder XRD pattern of $Ni_{50}Mn_{25+x}Sb_{25-x}$ ($x = 13$).

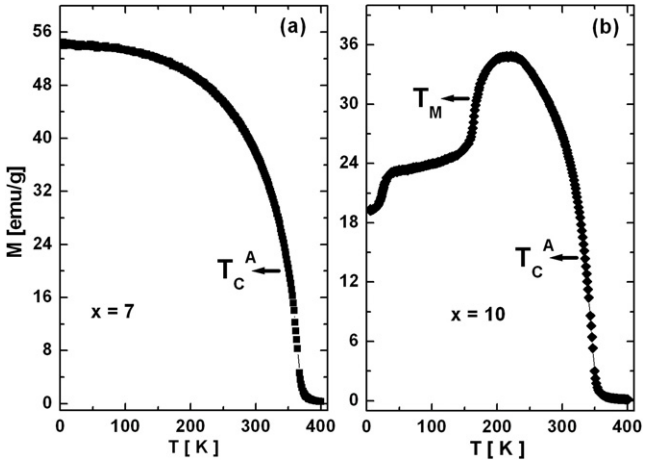

Figure 5. Magnetization as a function of temperature of $Ni_{50}Mn_{25+x}Sb_{25-x}$ (a) $x = 7$, and (b) $x = 10$, in an applied field of 1 kOe.

The calculated and observed room temperature XRD patterns of $Ni_{50}Mn_{25+x}Sb_{25-x}$ ($x = 13$) are presented in figure 3. The cross symbol represents the observed pattern and the solid line represents the calculated pattern. There is a very good agreement between the calculated and observed XRD patterns. Based on this agreement it was concluded that the $Ni_{50}Mn_{25+x}Sb_{25-x}$ ($x = 13$) alloy possesses an orthorhombic structure that belongs to the *Pmm2* space group. Similar XRD patterns were also obtained for the alloys with $x = 13.5$ and 14 (see figure 4). It was observed that the cell volumes of the austenitic phases in $Ni_{50}Mn_{25+x}Sb_{25-x}$ are smaller than the cell volumes of the martensitic phases (see table 1).

3.2. Magnetization

The magnetization curves as a function of temperature [$M(T)$] of $Ni_{50}Mn_{25+x}Sb_{25-x}$ for $x = 7$ and 10 in a field of 1 kOe are shown in figures 5(a) and (b), respectively. The only transition observed in the alloy with $x = 7$ was the ferromagnetic transition at $T_C^A = 362$ K (where the superscript A represents the austenitic phase). Although not shown, the $M(T)$ curves of the alloys with $x = 0$ and 6 were similar to that of the alloy with $x = 7$. In the $M(T)$ curve of the alloy with $x = 10$, a transition occurs near 25 K observed as a jump in the curve. At $T_M \approx 164$ K a sharp jump of magnetization was observed, which is a typical characteristic of the martensitic transition in a ferromagnetic state [8–11]. With further increase of temperature, a drop in magnetization occurs at the ferromagnetic transition temperature (T_C^A) of the austenitic phase.

The $M(T)$ curves of $Ni_{50}Mn_{25+x}Sb_{25-x}$ ($12 \leqslant x \leqslant 18$) at a field of 1 kOe are shown in figure 6. The $M(T)$ curves of the alloys with $12 \leqslant x \leqslant 13$ exhibit characteristics similar to that of the curve of the alloy with $x = 10$. However, in the $M(T)$ curve of the alloy with $x = 13$, a typical second-order transition around 255 K is observed. This transition represents the ferromagnetic transition (T_C^M) of the martensitic phase. Before the completion of the transition, a martensitic transformation occurs in the sample. Similar ferromagnetic transitions, although more subtle, are present for $x = 12$ and 12.5. As the Sb concentration decreases further, T_C^M becomes

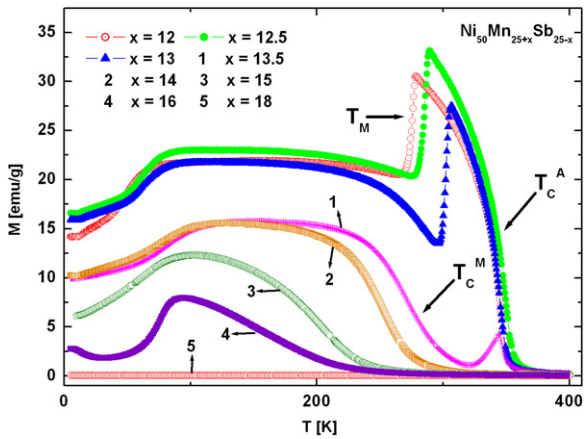

Figure 6. Magnetization as a function of temperature of $Ni_{50}Mn_{25+x}Sb_{25-x}$ ($12 \leqslant x \leqslant 18$) in an applied field of 1 kOe.

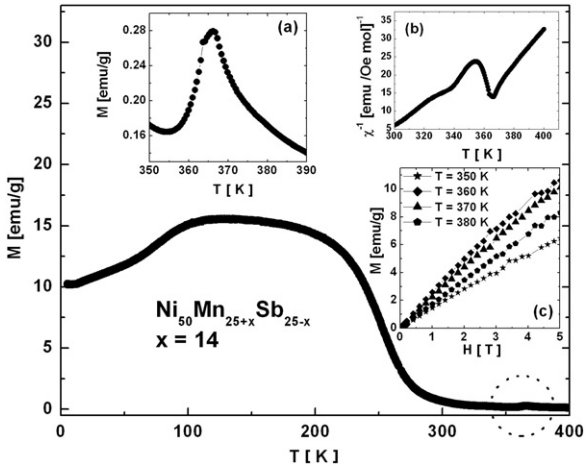

Figure 7. Magnetization as a function of temperature of $Ni_{50}Mn_{25+x}Sb_{25-x}$ for $x = 14$ in an applied field of 1 kOe. The insets show (a) the magnified version of the circled region, (b) the inverse susceptibility curve as a function of temperature, and (c) the magnetization as a function of field curves at temperatures near the observed transition.

more distinct, while the martensitic transition becomes less pronounced. In the $M(T)$ curve of the alloy with $x = 13.5$, the martensitic transformation is still observed in the form of a small jump in the magnetization around 336 K. The $M(T)$ curve of the alloy with $x = 14$–16 shows no martensitic transition in the ferromagnetic state, and the only transition observed is the ferromagnetic transition at T_C^M. The alloy with $x > 16$ shows no transition in the $M(T)$ curve. Figure 7 shows the $M(T)$ curve of $Ni_{50}Mn_{25+x}Sb_{25-x}$ with $x = 14$ obtained in a field of 1 kOe.

The insets (a), (b), and (c) show the $M(T)$ curves, inverse susceptibility, and $M(H)$ curves, respectively, of the circled region of figure 7. The magnified version of the circled region of figure 7 (inset (a)) shows a step-like transition near 361 K that resembles a typical antiferromagnetic transition. The inverse susceptibility curve, as shown in the inset (b) of figure 7, suggests the paramagnetic nature of the sample with

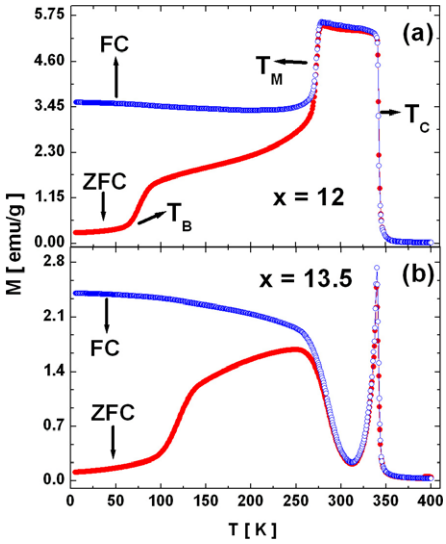

Figure 8. Zero field cooled and field cooled magnetization as a function of temperature of $Ni_{50}Mn_{25+x}Sb_{25-x}$ (a) $x = 12$ and (b) $x = 13.5$, in an applied field of 100 Oe.

$x = 14$. However, the slopes of the curves on each side of the transition at 361 K are different. The linearity of the $M(H)$ curves shown in inset (b) of figure 7 confirms that there is no observable ferromagnetism in the alloy with $x = 14$ near the transition at 361 K. These observations imply that the ferromagnetic regions of the alloy with $x = 14$ become paramagnetic during the ferromagnetic transition at T_C^M, while the antiferromagnetic regions become paramagnetic during the transition at 361 K. Figures 5–7 show evidence of the presence of some inhomogeneous magnetic state in the lower temperature regions (below 100 K) of $Ni_{50}Mn_{25+x}Sb_{25-x}$.

In order to understand this magnetic behavior, zero field cooled (ZFC) and field cooled (FC) magnetization measurements were performed. In figure 8, the ZFC and FC $M(T)$ curves of $Ni_{50}Mn_{25+x}Sb_{25-x}$ ($x = 12$, 13.5) alloys obtained in a field of 100 Oe are shown. The ZFC $M(T)$ curve of the alloy with $x = 12$ shows an increase in magnetization at around 65 K. This temperature is conventionally referred to as the exchange bias blocking temperature, T_B, below which the exchange bias effect is observed in the system [20]. With further increase of temperature the martensitic transformation is observed near 270 K, followed by a sharp drop in magnetization at the ferromagnetic transition temperature.

The only transitions observed in the FC $M(T)$ curve are the martensitic and the ferromagnetic transitions. Below T_M, the ZFC and FC curves split, demonstrating irreversible behavior. Such behaviors were also observed in the Ni–Mn–Sn and Ni–Mn–In Heusler alloy systems [11–13]. It was suggested that this type of behavior arises from the presence of both AFM and FM interactions in the system. The AFM interactions are consequences of the extra Mn atoms occupying the In/Sn sites that align antiparallely with the Mn on the Mn sites. Since the $Ni_{50}Mn_{25+x}Sb_{25-x}$ system is similar to those studied in [11–13], the splitting of the ZFC and FC $M(T)$ curves in $Ni_{50}Mn_{25+x}Sb_{25-x}$ is most probably due to the presence of AFM and FM interactions. The ZFC $M(H)$ curve

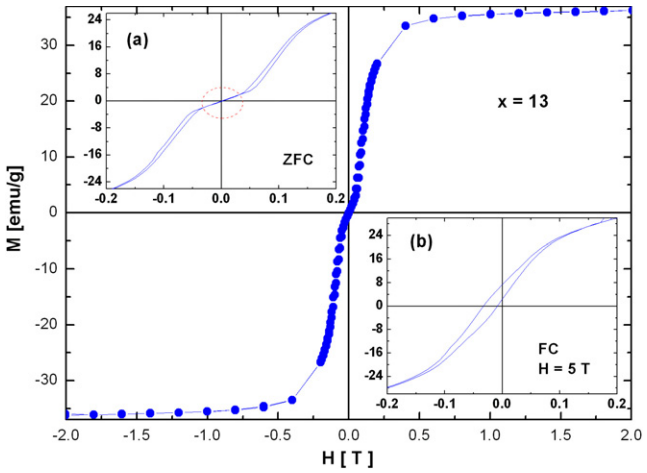

Figure 9. Magnetic hysteresis loop of $Ni_{50}Mn_{25+x}Sb_{25-x}$ ($x = 13$). The inset (a) shows the hysteresis loops from −0.2 T to 0.2 T and (b) shows the 5 T field cooled loop from −0.2 T to 0.2 T.

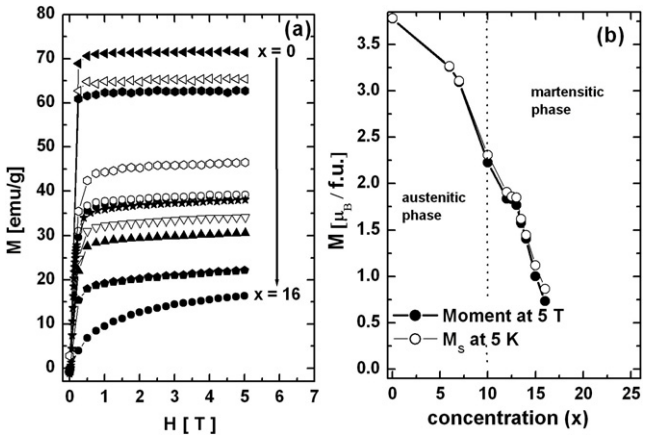

Figure 10. (a) Magnetization as a function of field of $Ni_{50}Mn_{25+x}Sb_{25-x}$ at 5 K. (b) The moment per Mn atom as a function of concentration x.

of the sample with $x = 13$, shown in figure 9, also suggests the presence of such interactions in the $Ni_{50}Mn_{25+x}Sb_{25-x}$ system.

As shown in the inset (a) of the figure, the alloy with $x = 13$ exhibits a double shifted hysteresis loop (hysteresis loops on each side of the circled region in the inset (a) of figure 9) when cooled in zero magnetic field. The double shifted loop no longer exists when the sample is cooled in the presence of a magnetic field of 5 T (see inset (b) of figure 9). The double shifted loops usually occur in exchange bias systems where there is an interface between AFM and FM regions [24–31]. A detailed discussion of the origin of such loops is given in [24]. Figure 10(a) shows the magnetization as a function of field of the $Ni_{50}Mn_{25+x}Sb_{25-x}$ system at 5 K. Figure 10(b) shows the magnetic moment at 5 T, and saturation magnetic moment, M_S, as a function of doping concentration (x) at 5 K. The moment at 5 T and the saturation moments are equal for $x \leqslant 7$, where the samples are in the austenitic phase at 5 K. For $x > 7$, the moments at 5 T are found to be less than the saturation moments. As shown in figure 10(b), the moments decrease with increasing Mn content. Theoretical

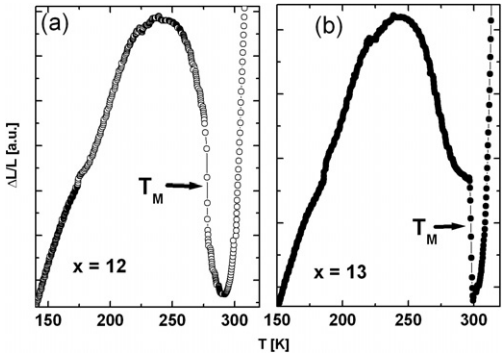

Figure 11. Thermal expansion curves of the alloys with (a) $x = 12$ and (b) $x = 13$.

and experimental investigations were conducted on Mn rich Ni_2MnGa [32]. Based on the computational results within the density-functional theory (DFT), it was shown that the moments of the extra Mn atoms align antiparallely with the moments of the other Mn atoms, and thus results in a decrease of the saturation magnetic moment of Ni_2MnGa. Based on this experimental evidence, it can be interpreted that moments of the Mn on the Sb sites of $Ni_{50}Mn_{25+x}Sb_{25-x}$ align antiparallely with the Mn atoms on the Mn sites. These antiparallel alignments cause a reduction in the total moment of the $Ni_{50}Mn_{25+x}Sb_{25-x}$ system, and the moment therefore depends almost linearly on doping concentration (x).

3.3. Thermal expansion and resistivity

The thermal expansion curves as a function of temperature of $Ni_{50}Mn_{25+x}Sb_{25-x}$ with $x = 12$ and 13 are shown in figures 11(a) and (b), respectively. The first-order nature of the martensitic transitions in $Ni_{50}Mn_{25+x}Sb_{25-x}$ is clearly seen as a discontinuity in these curves. Pronounced step-like changes in the thermal expansion curves at T_M indicate that the martensitic transition in $Ni_{50}Mn_{25+x}Sb_{25-x}$ is a first-order transition.

In order explore the electrical properties of $Ni_{50}Mn_{25+x}Sb_{25-x}$, electrical resistivity measurements were performed on some of the alloys in the series. Electrical resistivity is also an effective method of identifying the order of both magnetic and structural transitions. Resistivity curves as a function of temperature of $Ni_{50}Mn_{25+x}Sb_{25-x}$ with selected concentration (x) are shown in figure 12. For the sample with $x = 7$, no transition is observed in the resistivity curves except for a minor slope change near T_C. At the martensitic transition temperatures of the samples with $x \geqslant 13$, sharp drops in resistivity were observed. A resistivity drop of approximately 25% is observed in the $Ni_{50}Mn_{25+x}Sb_{25-x}$ alloys. Such sharp and significant step-like drops of the resistivity at T_M are also evidence of the first-order nature of the martensitic transformation in these alloys. Such characteristics of the resistivity curves at T_M are not observed in Ni–Mn–Ga based Heusler alloys [8]. The alloy with $x = 18$ shows no transition in the $R(T)$ curves, which is consistent with the $M(T)$ curve of the alloy (see figure 6).

Figure 13 shows the resistivity curves for the alloy with $x = 13$ at zero field and 5 T applied field. The figure

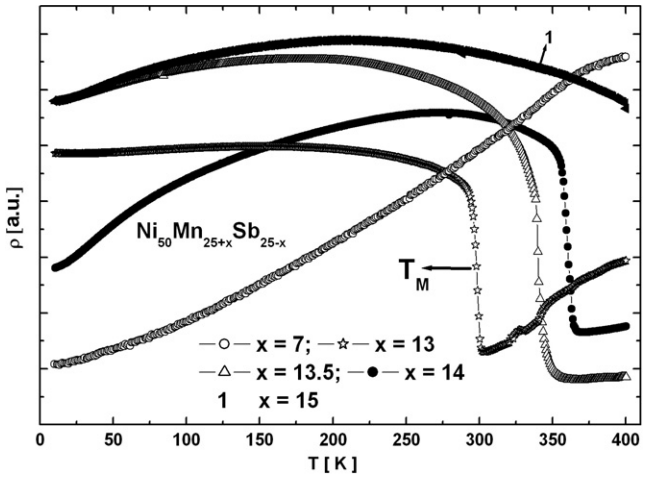

Figure 12. Resistivity as a function of temperature of $Ni_{50}Mn_{25+x}Sb_{25-x}$ ($7 \leqslant x \leqslant 15$).

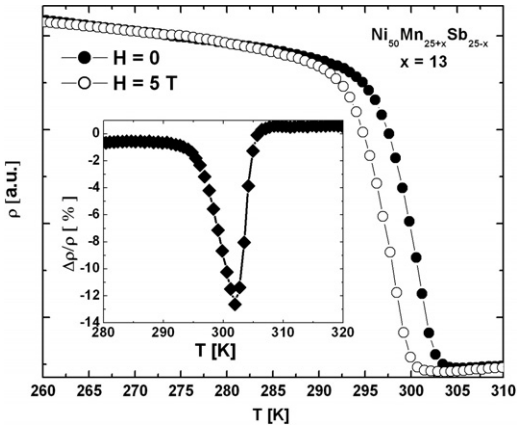

Figure 13. Resistivity as a function of temperature of $Ni_{50}Mn_{25+x}Sb_{25-x}$ for $x = 13$ in 0 and 5 T field. The inset shows the magnetoresistance as a function of temperature.

clearly reveals that martensitic transition occurs at a lower temperature in the 5 T field, and that there is approximately a 4 K difference in the martensitic transformation temperature obtained in 0 and 5 T fields. A magnetoresistance of −13.5% was observed in the alloy for a field change of 5 T (see inset of figure 10). The resistivity curves as a function of temperature in the $Ni_{50}Mn_{25+x}Sb_{25-x}$ system are very similar to those observed in $Mn_2Sb_{1-x}Sn_x$ and other metamagnetic systems, where an abrupt increase of electrical resistivity below the AF ordering temperature occurs due to a large decrease of the density of states (DOS) near the Fermi level [33–36]. Therefore it is possible that the martensitic transformation in the $Ni_{50}Mn_{25+x}Sb_{25-x}$ system is accompanied by an antiferromagnetic transition.

The resistivity curves for the alloy with $x = 13$ at 0 and 5 T field shown in figure 13 indicate that the martensitic transition temperature (T_M) is reduced by 4 K due to the application of a magnetic field of 5 T. The reduction of resistance near the antiferromagnetic transition temperature by the application of a magnetic field is also a typical characteristic of an antiferromagnetic

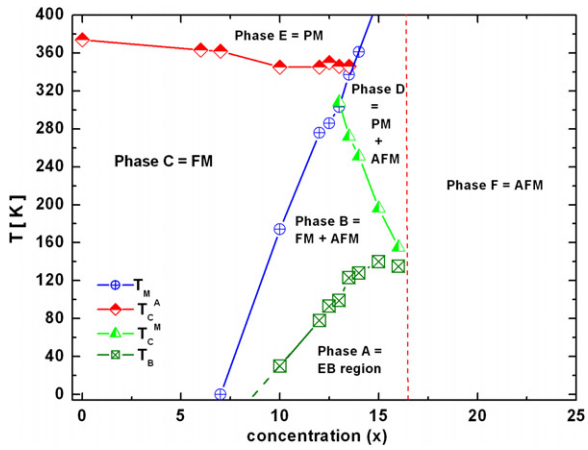

Figure 14. T–x phase diagram showing different magnetic regions of the $Ni_{50}Mn_{25+x}Sb_{25-x}$ system.

system. This interpretation can also be justified from the magnetization curves as a function of temperature of the alloy with $x = 14$ presented in figure 7. Although no martensitic transformation was observed in this curve, a typical antiferromagnetic type transition is observed at 361 K. At this same temperature a sharp change in resistance was observed in the resistivity of the alloy (see figure 12). The other alloys in the $Ni_{50}Mn_{25+x}Sb_{25-x}$ series that undergo martensitic transformations in a ferromagnetic state also exhibit similar characteristics in the resistivity. These observations strongly suggest that an antiferromagnetic transition is the main cause of the abrupt change in resistivity at the martensitic transformation temperature of $Ni_{50}Mn_{25+x}Sb_{25-x}$.

4. Discussion

The exchange bias blocking temperatures (T_B), martensitic transformation temperatures (T_M), ferromagnetic transition temperatures of the martensitic phase (T_C^M), and ferromagnetic transition temperatures of the austenitic phase (T_C^A), all as a function of doping concentration (x), are plotted in figure 14. As shown in the figure, with increasing Mn concentration the $T_C^{A'}$s were found to decrease. For $x < 10$ no martensitic transformation was observed in the $Ni_{50}Mn_{25-x}Sb_{25-x}$ system and the samples were found to possess the ferromagnetic cubic phase in the entire temperature region from 5–400 K. The martensitic transformation starts appearing in the sample with $x \geqslant 10$ and, with increasing Mn concentration, the martensitic transformation temperatures are found to increase.

The ferromagnetic transitions of the martensitic phase start appearing in the sample with $x = 13$, and T_C^M is found to decrease with increasing Mn concentration. When the Mn atoms in Ni_2MnGa are partially replaced by Cu or Co atoms, the electron concentration of the alloy increases, resulting in an increase of T_M [37]. In light of this observation, it can be suggested that the increase of T_M in the $Ni_{50}Mn_{25-x}Sb_{25-x}$ system with increasing Mn concentration is due to the increase of the electron concentration of the system.

Figure 14 also shows the various magnetic regions of the $Ni_{50}Mn_{25-x}Sb_{25-x}$ alloy system. The experimental data of the

system suggests that, depending on the doping concentration, six different magnetic regions exist in the system. Phase A is the EB region where AFM and FM regions exist in the $Ni_{50}Mn_{25-x}Sb_{25-x}$ system. It exists in the samples in the concentration range $x \geqslant 10$. Phase B is the mixed region where both ferromagnetic and antiferromagnetic (FM + AFM) martensitic phases coexist. This phase exists below T_M in the samples with concentration (x) ranging from 10 to 13, and below T_C^M in the samples with concentration (x) ranging from 13 to 14. Phase C is the ferromagnetic (FM) austenitic phase that exists for the samples in the concentration range $0 \leqslant x \leqslant 13$. In this concentration region, the system is found to be ferromagnetic above T_M and below T_C^A. Below T_M, both ferromagnetism and antiferromagnetism are found to coexist in the system. Phase D contains the paramagnetic and antiferromagnetic (PM + AFM) martensitic phases, and exists above T_C^M and below T_M in samples with $x > 13$. Phase E is the paramagnetic austenitic phase (PM) that exists above T_C^A in the samples with concentration range $0 \leqslant x \leqslant 13.5$, and above T_M in the samples with $x > 13$. The samples with $x > 16$ showed no transitions in the $M(T)$ curve. This behavior could be attributed to the fact that, for $x > 16$, the $Ni_{50}Mn_{25+x}Sb_{25-x}$ alloys become very similar to $Ni_{50}Mn_{50}$, which is antiferromagnetic with T_N more than 600 K [38]. Thus it can be suggested that for $x > 16$ the $Ni_{50}Mn_{25+x}Sb_{25-x}$ alloys are antiferromagnetic over the entire temperature range from 5–400 K. This is represented by Phase F in figure 14.

5. Conclusion

We have investigated the structural, magnetic, and electrical properties of the Heusler alloys $Ni_{50}Mn_{25+x}Sb_{25-x}$ ($0 \leqslant x \leqslant 18$). Martensitic transformations were observed in the alloys for some critical Sb concentration range. The austenitic phases are found to possess the $L2_1$ cubic structure, while the martensitic phases possess orthorhombic structures. It was found that the replacement of the Sb atoms by Mn atoms results in a decrease in the total magnetic moment of the system. Abrupt changes in resistivity were observed at the respective martensitic transformation temperatures. Supported by the magnetization measurements, it is likely that the abrupt change in resistivity at T_M is caused by an antiferromagnetic transition. As the Mn concentration increases, the T_C^M of the martensitic phase, and the T_C^A of the austenitic phase decreases, whereas the martensitic transformation temperature increases.

Acknowledgments

This research was supported by the Research Opportunity Award from Research Corporation (RA0357), and by the Office of Basic Energy Sciences, Material Sciences Division of the US Department of Energy (contract No. DE-FG02-06ER46291).

References

[1] Acet M, Duman E, Wassermann E F, Mañosa L and Planes A 2002 *J. Appl. Phys.* **92** 3867
[2] Li J Q, Liu Z H, Yu H C, Zhang M, Zhou Y Q and Wu G H 2003 *Solid State Commun.* **126** 323
[3] Wolter A U B, Bosse A, Baabe D, Maksimov I, Mienert D, Klauß H H, Litterst F J, Niemeier D, Michalak R, Geibel C, Feyerherm R, Hendrikx R, Mydosh J A and Süllow S 2002 *Phys. Rev.* B **66** 174428
[4] Plogmann S, Schlathölter T, Braun J, Neumann M, Yarmoshenko Yu M, Yablonskikh M V, Shreder E I, Kurmaev E Z, Wrona A and Slebarski A 1999 *Phys. Rev.* B **60** 6428
[5] Kubler J, Williams A R and Sommers C C 1983 *Phys. Rev.* B **28** 1745
[6] Ullakko K, Huang J K, Kantner C, O'Handley R C and Kokorin V V 1996 *Appl. Phys. Lett.* **69** 1966
[7] Khan M, Dubenko I, Stadler S and Ali N 2004 *J. Phys.: Condens. Matter* **16** 5259–66
[8] Khan M, Stadler S, Craig J, Mitchell J and Ali N 2006 *IEEE Trans. Magn.* **42** 3108
[9] Matsumoto M, Takagi T, Tani J, Kanomata T, Muramatsu N and Vasil'ev A N 1999 *Mater. Sci. Eng.* A **273–275** 326–8
[10] Sutou Y, Imano Y, Koeda N, Omori T, Kainuma R, Ishida K and Oikawa K 2004 *Appl. Phys. Lett.* **85** 4358
[11] Krenke T, Acet M, Wassermann E F, Moya X, Mañosa L and Planes A 2005 *Phys. Rev.* B **72** 014412
[12] Moya X, Mañosa L, Planes A, Krenke T, Acet M and Wassermann E F 2006 *Mater. Sci. Eng.* A **438–440** 911
[13] Krenke T, Acet M, Wassermann E F, Moya X, Mañosa L and Planes A 2006 *Phys. Rev.* B **73** 174413
[14] Koyama K, Okada H, Wantanabe K, kanomata T, Kainuma R, Ito W, Oikawa K and Ishida K 2006 *Appl. Phys. Lett.* **89** 182510
[15] Khan M, Ali N and Stadler S 2007 *J. Appl. Phys.* **101** 053919
[16] Krenke T, Duman E, Acet M, Wassermann E F, Moya X, Mañosa L and Planes A 2005 *Nat. Mater.* **4** 450–4
[17] Sharma V K, Chattopadhyay M K, Shaeb K H B, Chouhan A and Roy S B 2006 *Appl. Phys. Lett.* **89** 222509
[18] Han Z D, Wang D H, Zhang C L, Xuan H C, Gu B X and Du Y W 2007 *Appl. Phys. Lett.* **90** 042507
[19] Han Z D, Wang D H, Zhang C L, Tang S L, Gu B X and Du Y W 2006 *Appl. Phys. Lett.* **89** 182507
[20] Khan M, Dubenko I, Stadler S and Ali N 2007 *Appl. Phys. Lett.* **91** 072510
[21] Kraus W and Nolze G 1996 Windows version of PowderCell 1.0, a program for manipulation of crystal structures and calculation of the corresponding powder diffraction patterns *J. Appl. Crystallogr.* **29** 301
[22] Rodrigues-Carvajal J 1993 *Physica* B **192** 55
[23] Steinitz M O, Genossar J, Schnepfand W and Tindall D A 1986 *Rev. Sci. Instrum.* **57** 297
[24] Brück S, Sort J, Baltz V, Surinach S, Munoz J S, Dieny B, DolorsBaro M and Nogues J 2005 *Adv. Mater.* **17** 2978
[25] Miltényi P, Gierlings M, Bamming M, May U, Güntherodt G, Nogués J, Leighton C and Schuller I K 1999 *Appl. Phys. Lett.* **75** 2304
[26] Gökemeijer N J, Cai J W and Chien C L 1999 *Phys. Rev.* B **60** 3033
[27] Zhao H W, Wang W N, Wang Y J, Zhan W S and Xiao J Q 2002 *J. Appl. Phys.* **91** 6893
[28] Lai C H, Chen S A and Huang J C A 2000 *J. Magn. Magn. Mater.* **209** 122
[29] Chien C L, Gornakov V S, Nikitenko V I, Shapiro A J and Shull R D 2003 *Phys. Rev.* B **68** 014418
[30] Roshchin I V, Petracic O, Morales R, Li Z-P, Batlle X and Schuller I K 2005 *Europhys. Lett.* **71** 297
[31] Kirk T L, Hellwig O and Fullerton E E 2002 *Phys. Rev.* B **65** 224426

[32] Enkovaara J, Heczko O, Ayuela A and Nieminen R M 2003 *Phys. Rev.* B **67** 212405
[33] Zhang Y-q and Zhang Z-d 2003 *Phys. Rev.* B **67** 132405
[34] Fukuda H, Fujii H and Kamura H 2001 *Phys. Rev.* B **63** 054405
[35] Chan J Y and Kauzlarich S M 1998 *Phys. Rev.* B **57** R8103
[36] Wijngaard J H, Haas C and de Groot R A 1992 *Phys. Rev.* B **45** 5395
[37] Khan M, Doubenko I, Stadler S and Ali N 2005 *J. Appl. Phys.* **97** 10M304
[38] Kasper J S and Kouvel J S 1959 *J. Phys. Chem. Solids* **11** 231–8